Whole-Body MPC and Online Gait Sequence Generation for Wheeled-Legged Robots

Marko Bjelonic, Ruben Grandia, Oliver Harley, Cla Galliard, Samuel Zimmermann and Marco Hutter

Abstract— The additional degrees of freedom and missing counterparts in nature make designing locomotion capabilities for wheeled-legged robots more challenging. We propose a whole-body model predictive controller as a single task formulation that simultaneously optimizes wheel and torso motions. Due to the real-time joint velocity and ground reaction force optimization based on a kinodynamic model, our approach accurately captures the real robot's dynamics and automatically discovers complex and dynamic motions cumbersome to hand-craft through heuristics. Thanks to the single set of parameters for all behaviors, whole-body optimization makes online gait sequence adaptation possible. Aperiodic gait sequences are automatically found through kinematic leg utilities without the need for predefined contact and lift-off timings. Also, this enables us to reduce the cost of transport of wheeled-legged robots significantly. Our experiments demonstrate highly dynamic motions on a quadrupedal robot with non-steerable wheels in challenging indoor and outdoor environments. Herewith, we verify that a single task formulation is key to reveal the full potential of wheeled-legged robots.

I. INTRODUCTION

Quadrupedal robots are fast becoming more common in industrial facilities [1], and it is only a matter of time until we see more of these robots in our daily lives. The current pandemic [2] is accelerating this progress. Their locomotion capabilities are well understood, and there are many different approaches published that exploit knowledge about their natural counterparts [3], [4]. The understanding of locomotion principles has led to simplified models and heuristics that are widely used as templates to control legged robots [5]–[9]. While legged robots have already made their way into real-world applications, wheeled-legged robots are still (mostly) only within the research community [6], [10]–[19]. The locomotion capabilities of wheeled-legged robots are less understood since there are no natural counterparts. Due to the youth of the field, the research community is experimenting with novel simplifications that capture the dynamics of *hybrid locomotion*, i.e., simultaneous walking and driving. The additional degrees of freedom (DOF), however, make these simplified models cumbersome to design.

Hybrid locomotion for robots, such as depicted in Fig. 1, faces two specific problems, one requires *discrete*, and the other *continuous* decision making. The former relates to the task of finding the appropriate gait sequencing, i.e.,

Fig. 1. Our quadrupedal robot ANYmal [21], equipped with four non-steerable and torque-controlled wheels, is exploring indoor and outdoor environments. With our novel whole-body MPC, the robot achieves highly dynamic motions at speeds of up to 4 m/s, while gait sequences are automatically discovered for this complex hybrid platform. First row: Locomotion in high grass and over steep hills. Second row: Blind locomotion over a 0.20 m high step (32 % of leg length) and stairs with a 0.175 m high step (28 % of leg length). Third row: Pacing gait and 0.28 m high jump with front legs.

sequences of lift-off and touch-down timings, which becomes difficult to handcraft. Besides, the work in [20] reveals that the proper choice of gait sequences is crucial to reducing the cost of transport (COT). The latter describes the task of finding the continuous motion of the robot, i.e., the trajectories of the torso and the feet (or wheels). Our whole-body model predictive control (MPC) requires minimal assumptions about the robot's dynamics and kinematics, allowing us to propose an online gait sequence generation for wheeled quadrupedal robots.

A. Related Work

In the following sections, we categorize existing approaches to legged locomotion and bring them into the context of hybrid locomotion.

1) Discrete Decision Making: Gaits in legged robots are often hand-tuned and time-based. Moreover, appropriate

sequences of contact timings become hard to design when it comes to wheeled-legged robots, as shown in Fig. 1.

Mixed-integer optimization problems can solve the combinatorial complexity of foot-placement and there are a few approaches that run these algorithms on a real robot [22], [23]. In practice, however, these approaches plan footholds and contact timings in one optimization while the torso trajectory is optimized as a separate task. The work in [24] proposes a phase-based end-effector parameterization for simultaneously optimizing gait and motion. The optimization problem, however, becomes prone to local minima and, as such, depends on a good initialization. A learning-based scheme for the initialization of the nonlinear programming (NLP) based on offline experience is proposed to solve this problem [25]. In contrast, the work in [26] presents a contact invariant trajectory optimization formulation to synthesize motions for legged robots. These approaches have in common that their algorithms are currently impractical to run online on the real robot. The synergistic relationship between local model-based control, global value function learning, and exploration might be the first step towards online planning of these higher dimensional optimization problems [27].

Finding gait sequences in a separate task might reduce the problem's complexity and make online execution on the robot feasible. By considering the impulses that can be delivered by the legs, online gait adaptation is shown by the *MIT Cheetah* robot [28]. The authors, however, reduce the problem to 2D, due to the computational complexity of the 3D case. Motions of the torso and feet are found in decomposed tasks. The work in [29], on the other hand, uses a sampling-based method to find hybrid stepping paths. Here, the authors carefully hand-tune heuristics that guide the solver towards slow and static motions.

2) Continuous Decision Making: A *decomposed task approach* splits the problem into separate foot (or wheel) and torso tasks. By breaking down locomotion planning for high-dimensional (wheeled-)legged robots into two lower-dimensional sub-tasks, we hypothesize that the individual problems become more tractable. The coordination of each task's solution is one of the main challenges, and heuristics are needed to align the foot and torso motions. Many approaches were developed over the last years exploiting these task synergies [5]–[9], [17], [20], [30]–[33].

In contrast, a *single task approach* treats the continuous decision problem as a whole without breaking down the problem into several sub-tasks. Here, the challenge is to solve the problem in a reasonable time, so that online execution on the real robot becomes feasible. In the last few years, traditional legged locomotion research experienced a large amount of pioneering work in the field of MPC that now reliably runs on quadrupedal robots, like *ANYmal* [34], [35], and *MIT Cheetah* [36]. Another class of single task optimization problems involves trajectory optimization (TO) that precomputes complex trajectories over a time horizon offline. The work in [24] shows a single TO formulation for legged locomotion that automatically determines whole-body trajectories over non-flat terrain. Hybrid locomotion platforms, e.g., *Skaterbots* [19], [37] and walking excavators [38], provide a similar approach to motion planning over flat terrain by solving a NLP problem. Recent advances in learning-based locomotion show impressive results using reinforcement learning (RL) [39], where a single task is learned in an accurate simulation environment. The work in [40] presents an imitation learning approach where MPC solutions guide a policy search method.

The following two sections discuss the importance of dynamic models and foothold heuristics in the context of continuous decision making.

3) Dynamic models: Optimization-based methods depend on the choice of model complexity. Each dynamic model comes with its assumptions. For example, the linear inverted pendulum (LIP) model controls only the motion of the center of mass (COM) position and acts as a substitute for the contact forces. Here, the zero-moment point (ZMP) [41], or the center of pressure (COP), is constrained to lie inside the support polygon [5], [9], [15], [20], [31], [31], [42], [43]. These approaches result in fast update rates at the cost of inaccurate modeling of the real robot.

The real model can be approximated more accurately with a single rigid body dynamics (SRBD) model, which assumes that the joint accelerations' momentum is negligible and that the full system's inertia remains similar to some nominal configuration. Recent years showed impressive results, and many different research groups have adopted this more complex model [24], [32], [34], [36], [44].

Finally, the rigid body dynamics model only assumes non-deformable links, and by expressing the change of momentum in a frame fixed at the current COM, the equations of motion (EOM) can be rewritten as the Centroidal dynamics model without loss of generality [45]. Such a dynamic model is common in TO and provides a general approach to hybrid locomotion [19], [37]. Due to the increased complexity, these approaches are impractical to update online in a receding horizon fashion.

4) Foothold heuristics: As described in Section I-A.2, a decomposed task approach is completed in two stages, where a heuristic is needed to connect the feet and torso planning stages. For example, a common method in legged locomotion designs foothold positions based on the Raibert heuristic [46] with a capture-point-based feedback term [47]. In some work, this approach is also referred to as inverted pendulum models [5], [20]. The work in [36] regularizes a single task MPC using such kinds of heuristics. The question arises if these heuristics guide the optimization problem towards sub-optimal solutions due to the heuristic's simplicity.

B. Contribution

We extend the related work with a novel *gait sequence generation* and *whole-body MPC*. The former is responsible for generating discrete decisions about the contact and lift-off timings, while the latter is a single task approach, solving the task of findings continuous motions for the robot's torso and wheels. Moreover, the whole-body MPC optimizes the

real-time joint velocity and ground reaction force simultaneously and integrates a kinodynamic model of a wheeled quadrupedal robot. Our framework extends the capabilities of wheeled-legged robots in the following ways:

1) A single task approach, without needless heuristics, enables the robot to automatically discover complex and dynamic motions that are impossible to hand-tune.

2) Due to the kinodynamic model, our framework accurately captures the real robot's dynamics and improves the prediction accuracy.

3) Our whole-body MPC is general enough to perform all behaviors with the same set of parameters, enabling flexibility with respect to (w.r.t.) the gait sequence.

4) We also propose a novel concept to quantify kinematic leg utilities for online gait sequence generation without the need for predefined contact timings and lift-off sequences. The automatic gait discovery enables wheeled quadrupedal robots, as depicted in Fig. 1, to coordinate aperiodic behavior.

Fig. 2 visualizes our complete locomotion controller that is verified in challenging indoor and outdoor environments. In the following, we introduce the main contributions, the gait sequence generation and whole-body MPC, in more detail.

II. GAIT SEQUENCE GENERATION

Gait timings and their sequences are discovered through a kinematic utility of each leg. Given an external reference trajectory[1] $\boldsymbol{r}_{B,\mathrm{ref}}(t)$ of the torso B, aperiodic sequences of

[1]The reference trajectory is generated from an external source, e.g., an operator device or a navigation planner. In case of reference velocities, i.e., the linear velocity vector of the COM $\boldsymbol{v}_{\mathrm{ref}}$ and the angular velocity vector $\boldsymbol{\omega}_{\mathrm{ref}}$, the reference trajectory can be computed by integrating the reference velocity reference.
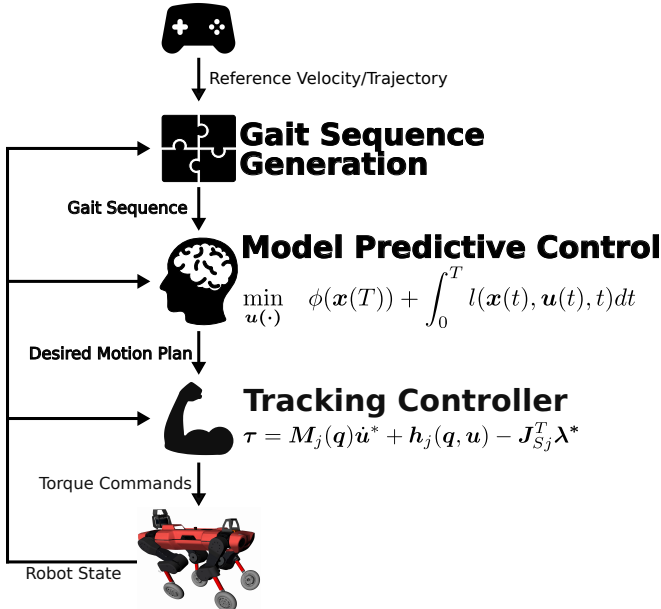

Fig. 2. Overview of the locomotion controller. The gait sequence generator automatically transforms reference trajectories from a higher-level planner or operator device into lift-off and touch-down sequences. These gait sequences are fed into the MPC that optimizes joint velocities and contact forces over a time horizon T. Finally, a tracking controller, e.g., [15], transforms the desired motion plan into torque references $\boldsymbol{\tau}$.

contact and lift-off timings are generated over a time horizon T.

A. Kinematic Leg Utility

For the robot to locomote, i.e., drive or walk, it needs to have a sense of each leg's utility $u_i(t) \in [0, 1]$. If the utility of one leg approaches zero, the leg needs to be recovered by a swing phase. In contrast to [28], where the utility is based on impulse generation capabilities and used as a metric for a decomposed task approach, we propose that the kinematic capability is of primary importance for gait adaptation of a single task approach. This utility quantifies the usefulness of a leg in terms of remaining in kinematic reach.

Wheeled quadrupedal robots with non-steerable wheels, as shown in Fig. 1, have a fixed rolling direction. While in contact, the trajectory of the wheel $\boldsymbol{r}_{E_i,\mathrm{ref}}(t) = \boldsymbol{r}_{E_i} + \pi_{E_i,\parallel}(\boldsymbol{r}_{B,\mathrm{ref}}(t))$ is kinematically constrained, where $\boldsymbol{r}_{E_i}$ is the measured position of wheel i for end-effector[2] E_i, and $\pi_{E_i,\parallel}(\cdot)$ projects a vector onto the rolling direction of wheel E_i, while $\pi_{E_i,\perp}(\cdot)$ projects a vector onto the lateral direction of the rolling direction.

By defining the utility as an ellipse, we can distinguish the decay along and lateral to the rolling direction. Therefore, the leg's utility $u_i(t) \in [0, 1]$ is defined as

$$u_i(t) = 1 - \sqrt{\left(\frac{\pi_{E_i,\parallel}(\widetilde{\boldsymbol{r}}_{E_i}(t))}{\lambda_{\parallel}}\right)^2 + \left(\frac{\pi_{E_i,\perp}(\widetilde{\boldsymbol{r}}_{E_i}(t))}{\lambda_{\perp}}\right)^2},$$
(1)

where the position error is given by $\widetilde{\boldsymbol{r}}_{E_i}(t) = \boldsymbol{r}_{B,\mathrm{ref}}(t) + \boldsymbol{r}_{BD_i} - \boldsymbol{r}_{E_i,\mathrm{ref}}(t)$, and $\boldsymbol{r}_{BD_i}$ is the position from the torso B to the recent contact position at touch-down D_i of leg i. $\lambda_{\parallel}$ and $\lambda_{\perp}$ are the two half-axis lengths of the ellipse along and lateral to the rolling direction, respectively.

B. Gait Timings Generation

The leg remains in contact as long as its utility $u_i(t)$ remains above a certain threshold $\bar{u} \in [0, 1]$. If a leg's utility falls below the threshold, i.e., the leg is close to its workspace limits, then this leg is recovered by a swing phase with constant swing duration. Similar to [28], a multi-layered swing generator is proposed to achieve meaningful leg coordination:

1) *Utility generation*: Calculate the utility for all legs $u_i(t)$ over a time horizon T.

2) *Utility check*: Find the time t^* when $u_i(t) < \bar{u}$ and give legs with the lowest utility priority to add a swing phase with constant swing duration at time t^*.

3) *Neighboring legs check*: A swing phase is added if the neighboring legs[3] are not swinging. Otherwise, the swing phase is postponed until the neighboring legs are in contact. Such an approach constraints the gaits to pure driving, hybrid static, and hybrid trotting gaits.

[2]We let the frame E_i be fixed at a leg's endpoint, i.e., the point on the wheel that during stance is in contact with the ground, and define this point as a leg's end-effector. This enables us to model conventional point-foot and wheels simply by changing the kinematic constraints.

[3]For the left-front leg of a quadruped, the neighboring legs are the right-front and left-hind legs.

III. WHOLE-BODY MODEL PREDICTIVE CONTROL

The general MPC formulation is to find the control input that optimizes the following cost function over a receding horizon T

$$\underset{\boldsymbol{u}(\cdot)}{\text{minimize}} \quad \phi(\boldsymbol{x}(T)) + \int_0^T l(\boldsymbol{x}(t), \boldsymbol{u}(t), t)\mathrm{d}t,$$

$$\boldsymbol{x}(t) = \begin{bmatrix} \boldsymbol{\theta}^T & \boldsymbol{p}^T & \boldsymbol{\omega}^T & \boldsymbol{v}^T & \boldsymbol{q}_j^T \end{bmatrix}^T, \quad (2)$$

$$\boldsymbol{u}(t) = \begin{bmatrix} \boldsymbol{\lambda}_E^T & \boldsymbol{u}_j^T \end{bmatrix}^T,$$

where $\boldsymbol{x}(t) \in \mathbb{R}^{12+n_j}$ is the state vector and $\boldsymbol{u}(t) \in \mathbb{R}^{3n_e+n_j}$ is the control input vector at time t, with $n_j = 12$ is the number of joints and $n_e = 4$ is the number of legs. Note that the additional four DOF of the wheels are not explicitly in the state or input vector. More precisely, the wheel is modeled as a moving point contact, which later on is translated into wheel inputs by the tracking controller. The elements $\boldsymbol{\theta}$, $\boldsymbol{p}$, $\boldsymbol{\omega}$, $\boldsymbol{v}$ and $\boldsymbol{q}_j$ of the state vector refer to the orientation of the torso in Euler angles, the positions of the torso in world frame W, the angular rate of the COM, the linear velocity of the COM, and the joint positions, respectively. Moreover, the control inputs are the end-effector contact forces $\boldsymbol{\lambda}_E$ and joint velocities $\boldsymbol{u}_j$. Here, $l(\cdot)$ is the time-varying running cost, and $\phi(\cdot)$ is the cost at the terminal state $\boldsymbol{x}(T)$.

In addition to the cost function in (2), the system dynamics, initial condition, and further equality and inequality constraints need to be satisfied as given by

$$\dot{\boldsymbol{x}}(t) = \boldsymbol{f}(\boldsymbol{x}(t), \boldsymbol{u}(t), t), \quad (3a)$$

$$\boldsymbol{x}(0) = \boldsymbol{x}_0, \quad (3b)$$

$$\boldsymbol{g}_1(\boldsymbol{x}(t), \boldsymbol{u}(t), t) = 0, \quad (3c)$$

$$\boldsymbol{g}_2(\boldsymbol{x}(t), t) = 0, \quad (3d)$$

$$\boldsymbol{h}(\boldsymbol{x}(t), \boldsymbol{u}(t), t) \geq 0. \quad (3e)$$

The feedback policy is calculated using the sequential linear quadratic (SLQ) method, which is a differential dynamic programming (DDP) based algorithm for continuous-time systems. In particular, the method in [34] is being used which extends the SLQ formulation of [48] for use with inequality constraints. SLQ computes via quadratic approximations of the value function a time-varying, state-affine control policy through an iterative process. The state-input equality constraint (3c), the pure state equality constraint (3d), and the inequality constraint (3e) are handled by a Lagrangian method, a penalty method, and a relaxed barrier function, respectively. To accommodate compliant contacts and bandwidth limitations due to actuator dynamics, we include frequency-shaped cost functions to achieve robust solutions as introduced by [49]. In the following sections, the implementation of the cost function and constraints is described in more detail.

A. Cost Function

We are interested in tracking the reference trajectory $\boldsymbol{r}_{B,\mathrm{ref}}(t)$, and the difference of the state and control through a quadratic cost function given by

$$l(\boldsymbol{x}(t), \boldsymbol{u}(t), t) = \frac{1}{2}\boldsymbol{x}(t)^T \boldsymbol{Q} \boldsymbol{x}(t) + \frac{1}{2}\boldsymbol{u}(t)^T \boldsymbol{R} \boldsymbol{u}(t), \quad (4)$$

where $\boldsymbol{Q}$ and $\boldsymbol{R}$ are positive semi-definite Hessians of the state and control input vector, respectively.

B. Equations of Motion

The system's dynamics (3a) is based on a kinodynamic model of a wheeled quadrupedal robot. It defines the SRBD model along with the kinematics for each leg while treating the wheels as locked joints. SRBD assumes that the limb joints' momentum is negligible compared with the lumped COM inertia and the inertia of the full-body system stays the same as to some nominal joint configuration. The EOM of the SRBD is given by

$$\dot{\boldsymbol{\theta}} = \boldsymbol{T}(\boldsymbol{\theta})\boldsymbol{\omega}, \quad (5a)$$

$$\dot{\boldsymbol{p}} = \boldsymbol{R}_{WB}(\boldsymbol{\theta})\boldsymbol{v}, \quad (5b)$$

$$\dot{\boldsymbol{\omega}} = \boldsymbol{I}^{-1}\left(-\boldsymbol{\omega} \times \boldsymbol{I}\boldsymbol{\omega} + \sum_{i=1}^{n_e} \boldsymbol{r}_{E_i}(\boldsymbol{q}_j) \times \boldsymbol{\lambda}_{E_i}\right), \quad (5c)$$

$$\dot{\boldsymbol{v}} = \boldsymbol{g}(\boldsymbol{\theta}) + \frac{1}{m}\sum_{i=1}^{n_e} \boldsymbol{\lambda}_{E_i}, \quad (5d)$$

$$\dot{\boldsymbol{q}}_j = \boldsymbol{u}_j, \quad (5e)$$

where $\boldsymbol{R}_{WB}(\boldsymbol{\theta}) \in SO(3)$ represents the rotation matrix that projects the components of a vector from the torso frame B to the world frame W, $\boldsymbol{T}(\boldsymbol{\theta})$ is the transformation matrix from angular velocities in the torso frame B to the Euler angles derivatives in the world frame W, $\boldsymbol{I}$ is the moment of inertia of the COM taken at the nominal configuration of the robot, m is the total mass, $\boldsymbol{g}(\boldsymbol{\theta})$ is the gravitational acceleration in torso frame B, and, as described in the footnote of Section II-A, $\boldsymbol{r}_{E_i}(\boldsymbol{q}_j)$ is the end-effector's contact position of leg i with respect to the COM.

C. Rolling Constraint

The contact constraint of traditional legged robots is modeled though the end-effectors' velocities, and when in contact, these velocities are restricted to zero in all directions. Wheeled-legged robots, on the other hand, can execute motions along the rolling direction when in contact. Thus, the end-effector constraint of a leg i in contact is represented by

$$\boldsymbol{\lambda}_{E_i} \in C(\boldsymbol{n}, \mu_C),$$
$$\pi_{E_i, \perp}(\boldsymbol{v}_{E_i}) = 0, \quad (6)$$
$$\boldsymbol{v}_{E_i} \cdot \boldsymbol{n} = 0,$$

where $C(\boldsymbol{n}, \mu_C)$ and $\boldsymbol{n}$ are the friction cone presented in the next section and the local surface normal in world frame W, respectively. Due to the kinodynamic model of the whole-body, the projection $\pi_{E_i, \perp}(\cdot)$ of the end-effector velocity in world frame $\boldsymbol{v}_{E_i}$ onto the perpendicular direction of the rolling direction can be easily computed through forward kinematics. With this formulation, legs in contact are constrained, such that, the velocity along the rolling direction is left unconstrained, i.e, $\pi_{E_i, \parallel}(\boldsymbol{v}_{E_i}) \in \mathbb{R}$.

While leg i is in air, the constraint switches to

$$\begin{aligned}
\boldsymbol{\lambda}_{E_i} &= \mathbf{0}, \\
\boldsymbol{v}_{E_i} \cdot \boldsymbol{n} &= c(t),
\end{aligned} \tag{7}$$

where legs in the air follow a predefined swing trajectory $c(t)$ in the direction of the terrain normal $\boldsymbol{n}$ and the ground reaction forces $\boldsymbol{\lambda}_{E_i}$ are set to zero.

D. Friction Cone Constraint

As given in (6), the friction cone constraint $\boldsymbol{\lambda}_{E_i} \in C(\boldsymbol{n}, \mu_C)$ implements an inequality constraint which is given by

$$\mu_C F_z - \sqrt{F_x^2 + F_y^2} \geq 0, \tag{8}$$

where the local contact force $\boldsymbol{F} = \begin{bmatrix} F_x & F_y & F_z \end{bmatrix}^T$ is a projection of the ground reaction forces $\boldsymbol{\lambda}_{E_i}$ to the frame of the terrain surface given by $\boldsymbol{n}$, and μ_C is the friction coefficient.

IV. EXPERIMENTAL RESULTS AND DISCUSSION

We validate our whole-body MPC and gait sequence generation in several real-world experiments where we compare the performance of our approach with the motion planner introduced in [20]. It is based on a decomposed task approach, i.e., the wheel and torso trajectories are not solved in a single task optimization as presented here. To the best of our knowledge, this is the first time a study compares the performance of a single and decomposed task approach on the same robotic platform. Table I gives an overview of both approaches and lists the capabilities of both algorithms. Each element is described in more detail in the following sections, which reports on experiments conducted with ANY-mal equipped with non-steerable, torque-controlled wheels (see Fig. 1). The conclusions, however, can be generalized to any (wheeled-)legged robot. A video[4] showing the results accompanies this paper.

A. Experimental Setup

Our whole-body MPC, tracking controller, and state estimator run in concurrent threads on a single PC (Intel i7-8850H, 2.6 GHz, hexa-core 64-bit). The robot is entirely self-contained in terms of computation, and all optimization problems are run online due to fast solver times.

1) Tracking controller: The operational space reference motions of the whole-body MPC are tracked by a whole-body controller (WBC), which is based on the hierarchical optimization framework described in [15]. Desired torque commands $\boldsymbol{\tau}^*$ are generated for each actuator while accounting for the full rigid body dynamics, including its physical constraints, e.g., the non-holonomic rolling constraint, friction cone, and torque limits. Each constraint is formulated as a cascade of quadratic programming (QP) problems composed of linear equality and inequality tasks, which are solved in a strict prioritized order. In our work, instead of minimizing the contact forces, the optimized

TABLE I
CAPABILITIES OF OUR PRESENTED WHOLE-BODY MPC COMPARED TO OUR PREVIOUS PUBLICATION [20]. TABLE IS ADAPTED FROM [50].

	Whole-Body MPC	Decomposed Task [20]
Dynamic model (accuracy)	Kinodynamic model	ZMP model
Number of optimizations	Single optimization	Separate wheel and base optimization
Foothold heuristic	No heuristics	Inverted pendulum model
Update rate	20-40 Hz	100-200 Hz
Reliability	High	Medium
Maximum reliable speed	3.5 m/s	1.5 m/s
Accelerations	High	Low
Optimized components		
Base motion	6D	3D
Footholds	3D	2D
Swing leg motion	✓	✓
Contact force	✓	✗
Step timing/sequence	✗	✗
Difficulty of shown task		
Line contacts	✓	✓
Point contacts	✓	✓
Flight phases	✓	✓
Inclined terrain	✓	✓
Non-flat terrain	✓	✗
Step timing/sequence adaptation	✓	✗

contact forces of the whole-body MPC are being tracked on the lowest priority. Finally, the reference actuation torques are given by $\boldsymbol{\tau}_{ref} = \boldsymbol{\tau}^* + \boldsymbol{k}_P(\boldsymbol{q}_j^* - \boldsymbol{q}) + \boldsymbol{k}_D(\boldsymbol{u}_j^* - \dot{\boldsymbol{q}})$, where $\boldsymbol{k}_P$ and $\boldsymbol{k}_D$ are the gains of the joint-space position and velocity controller.

2) State estimation: We fuse the inertial measurement unit (IMU) readings and the kinematic measurements from each actuator to acquire the robot's state [51]. The robot is locally modeling the terrain as a three-dimensional plane, which is estimated by fitting a plane through the most recent contact locations [15]. Each leg's contact state is then determined by estimating the contact force, which considers the measurements of the motor drives and the full-rigid body dynamics. The state estimator and the WBC run together in a 400 Hz loop.

In the following, we use a fixed trotting gait and compare the two approaches' performance in terms of their prediction error, dynamic model, and foothold heuristic. The last section reports on results conducted in combination with the gait sequence generation.

B. Prediction Error

The optimization problem's ability to accurately predict the robot's state over a predefined time horizon is a crucial component. It gives us a measure of how accurate the underlying algorithm models the real system. In the following, we are defining the prediction error Δp_{pred} as follows

$$\Delta p_{\mathrm{pred}} = \|\boldsymbol{p}^*_{-T}(T) - \boldsymbol{p}_{\mathrm{meas}}\|, \quad \forall \boldsymbol{v}_{\mathrm{ref}}, \boldsymbol{\omega}_{\mathrm{ref}} = \mathrm{const.}, \tag{9}$$

where $\boldsymbol{p}^*_{-T}(T)$ is the terminal position of the COM optimized T s ago, and $\boldsymbol{p}_{\mathrm{meas}}$ is the measured position of the COM. Moreover, the prediction error is only computed for constant reference velocities $\boldsymbol{v}_{\mathrm{ref}}$ and $\boldsymbol{\omega}_{\mathrm{ref}}$.

Fig. 3 compares the performance of our whole-body MPC with the decomposed task approach described in [20]. Especially at higher commanded velocities, the prediction error of the whole-body MPC outperforms the prediction accuracy of our previously published controller, which is also prone to failures at higher speeds. Decoupling the locomotion problem into a wheel and torso task makes it untrackable at higher speeds. The actual wheel and base trajectories start to diverge and require an additional heuristic to maintain balance. Our single task approach, however, solves this problem and improves the prediction accuracy by up to 71 %, making fast locomotion feasible.

C. Dynamic Model

Various approaches use a LIP model that optimizes over the ZMP as a substitute for the contact forces. These approaches generate trajectories of the COM, so that the ZMP lies inside the support polygon spanned by the legs in contact. The question arises whether this approach accurately captures the real dynamics. Therefore, we are logging the
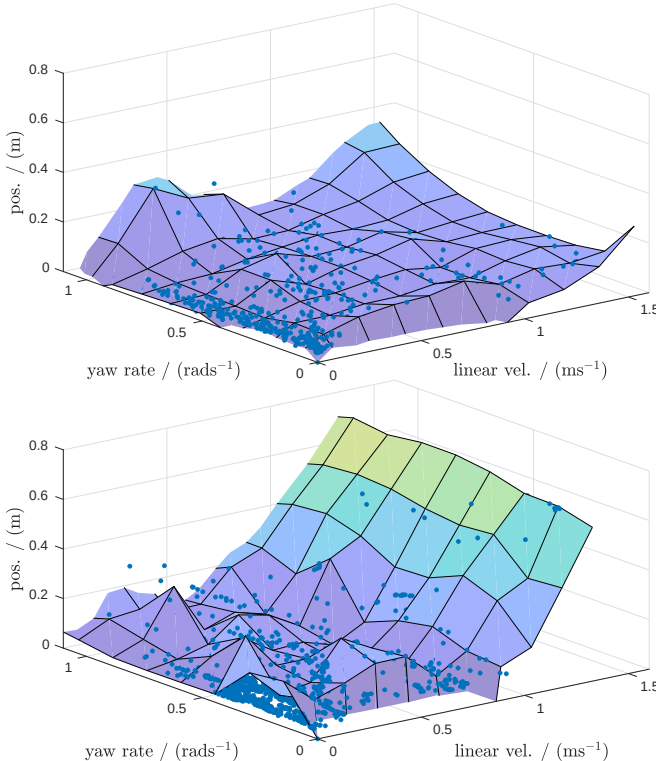

Fig. 3. Prediction error for $T = 0.8$s of the COM while hybrid trotting on flat terrain. The upper figure depicts the result of our proposed whole-body MPC, and the lower figure shows the result of our previously published decomposed task approach [20]. With our new locomotion controller, we achieve a prediction error of $\Delta p_{\mathrm{pred}} = 0.061 \pm 0.044$m which outperforms the result of the decomposed task approach with $\Delta p_{\mathrm{pred}} = 0.214 \pm 0.061$m. Our single task approach improves the prediction accuracy by approximately 71 %, which becomes evident at higher commanded linear velocities and yaw rates.

ZMP of [20] while running our whole-body MPC using a more realistic kinodynamic model of a wheeled-legged robot.

The result in Fig. 4 shows that while executing dynamical behavior, the ZMP diverges from the support polygon. Therefore, the ZMP model is not capable of discovering motions as depicted in Fig. 5, due to its simplifications. Furthermore, there is also one qualitative argument that speaks for a more accurate model as the kinodynamic model. The idea of the ZMP only holds in the presence of co-planar contacts [52], and as such, it can not accurately capture environments, as shown in the second row of Fig. 1.

D. Foothold Heuristic

While the whole-body MPC approach does not integrate any foothold heuristic, the decomposed task approach relies on the inverted pendulum model based on a feedforward and feedback part. The former aligns the motions with the reference trajectory while the latter corrects the foothold under different conditions, such as modeling errors, external disturbances, and transitions. Similar to the result in Section IV-C, Fig. 4 shows that the inverted pendulum
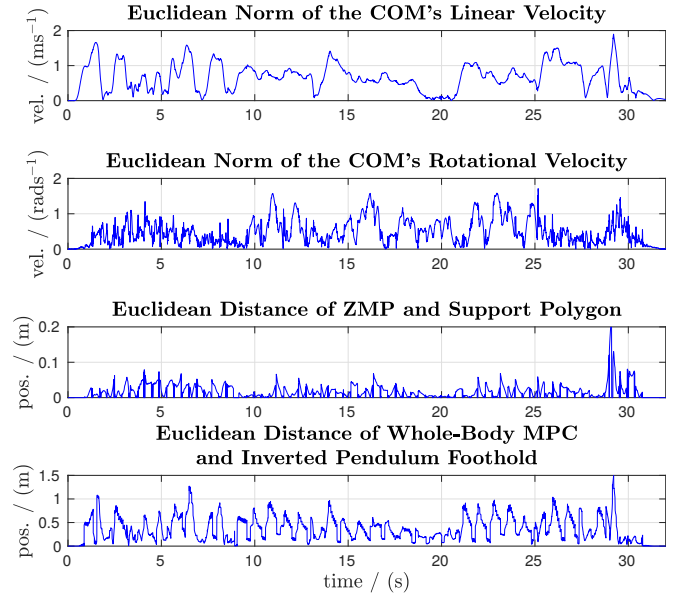

Fig. 4. Results of our whole-body MPC while commanding high base accelerations. The upper two figures show the plot of the commanded linear and rotational velocities. We compare the performance of the ZMP model in the third plot. These high accelerations are not feasible to achieve with such a model since the ZMP diverges from the support polygon, i.e., the robot is supposed to fall based on the ZMP theory. Similarly, the inverted pendulum model's heuristic starts diverging from our approach's complex behaviors (last plot).

Fig. 5. High accelerations using the whole-body MPC approach. The robot executes a fast change of direction between 2 and -2 m/s, which forces the optimization problem to find complex motions that can not be captured by simple heuristics.

model starts diverging from our optimized footholds at higher accelerations due to the assumption of a constant reference velocity of the torso, which is tried to be compensated through the feedback term. Besides, the inverted pendulum model adapts to unforeseen disturbances while stepping and is originally not designed for wheeled-legged robots. Handcrafting a heuristic that finds more dynamic and hybrid trajectories on the ground w.r.t. the work in [20] is cumbersome. Our approach discovers complex behaviors automatically, as depicted in Fig. 5 due to the single-task approach.

E. Gait Sequence Generation

Fig. 6 shows the result of the gait sequence generation in combination with the whole-body MPC. The plot shows three interesting time snippets where the robot executes high linear velocities in combination with no, medium, and high rotational velocities. The gait sequence generator based on kinematic leg utilities intuitively switches between pure driving, static gaits (three legs in contact), and a trotting gait. All in all, our approach enables wheeled-legged robots to reduce the total amount of unnecessary steps, lowering the COT [16].

One of the benefits of our whole-body MPC is that it uses one set of cost terms for each gait. By contrast, the decomposed task approach, as described in [5], [20], requires re-tuning the cost terms for each gait pattern. Therefore, it is not feasible to run our gait timings generator with such approaches without adding more heuristics that interpolate between sets of pre-tuned cost terms.

V. CONCLUSIONS

We present a novel gait sequence generation and whole-body MPC for wheeled-legged robots. The former is based on the generation of kinematic leg utilities and makes the need for predefined sequences of contact and lift-off timings obsolete. The whole-body MPC finds the robot's torso and wheels motion in a single task, where real-time joint velocity and ground reaction force are simultaneously being optimized based on a kinodynamic model. The experimental results verify that our approach improves the model's accuracy and enables the robot to automatically discover complex and highly dynamic motions that are impossible to find through hand-tuned heuristics. Due to the single set of parameters, the whole-body MPC is flexible w.r.t. the gait sequence. Our wheeled-legged robot ANYmal is now, for the first time, capable of coordinating aperiodic behavior, which decreases the overall COT of our missions.

In future work, we plan to incorporate the contact timings' optimization into the whole-body MPC. The biggest challenge remains the online execution of such a problem.

REFERENCES

[1] C. D. Bellicoso, M. Bjelonic, L. Wellhausen, K. Holtmann, F. Günther, M. Tranzatto, P. Fankhauser, and M. Hutter, "Advances in real-world applications for legged robots," *Journal of Field Robotics*, vol. 35, no. 8, pp. 1311–1326, 2018.

[2] BBC News. Coronavirus: Robot dog enforces social distancing in singapore park. BBC News. [Online]. Available: https://www.bbc.com/news/av/technology-52619568

[3] P. Eckert, A. Spröwitz, H. Witte, and A. J. Ijspeert, "Comparing the effect of different spine and leg designs for a small bounding quadruped robot," in *IEEE Int. Conf. on Robotics and Automation*, 2015, pp. 3128–3133.

[4] J. A. Nyakatura, K. Melo, T. Horvat, K. Karakasiliotis, V. R. Allen, A. Andikfar, E. Andrada, P. Arnold, J. Lauströer, J. R. Hutchinson, *et al.*, "Reverse-engineering the locomotion of a stem amniote," *Nature*, vol. 565, no. 7739, p. 351, 2019.

[5] C. D. Bellicoso, F. Jenelten, C. Gehring, and M. Hutter, "Dynamic locomotion through online nonlinear motion optimization for quadrupedal robots," *IEEE Robotics and Automation Letters*, vol. 3, no. 3, pp. 2261–2268, 2018.

[6] A. Laurenzi, E. M. Hoffman, and N. G. Tsagarakis, "Quadrupedal walking motion and footstep placement through linear model predictive control," in *IEEE/RSJ Int. Conf. on Intelligent Robots and Systems*, 2018, pp. 2267–2273.

[7] J. R. Rebula, P. D. Neuhaus, B. V. Bonnlander, M. J. Johnson, and J. E. Pratt, "A controller for the littledog quadruped walking on rough terrain," in *IEEE Int. Conf. on Robotics and Automation*, 2007, pp. 1467–1473.

[8] M. Focchi, R. Orsolino, M. Camurri, V. Barasuol, C. Mastalli, D. G. Caldwell, and C. Semini, *Heuristic Planning for Rough Terrain Locomotion in Presence of External Disturbances and Variable Perception Quality*. Springer International Publishing, 2020, pp. 165–209.

[9] F. Jenelten, T. Miki, A. E. Vijayan, M. Bjelonic, and M. Hutter, "Perceptive locomotion in rough terrain – online foothold optimization," *IEEE Robotics and Automation Letters*, vol. 5, no. 4, pp. 5370–5376, 2020.
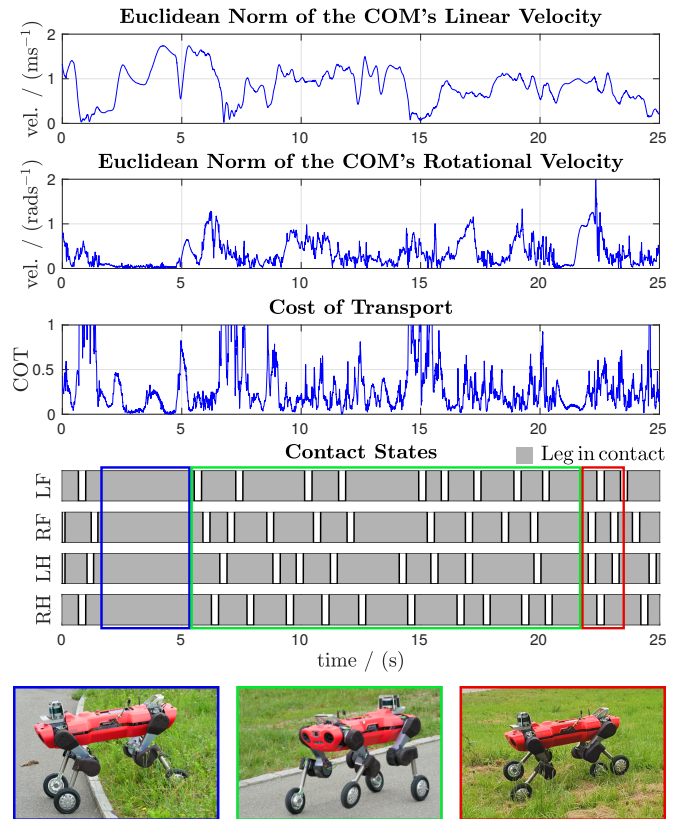
Fig. 6. Contact timings diagram while running the gait sequence generator and whole-body MPC. The two upper plots show the linear and rational velocity of the COM, the third plot depicts the mechanical COT [16], and the corresponding contact states are displayed in the four lower rows (left-front (LF), right-front (RF), left-hind (LH), and right-hind leg (RH)). The robot performs three different motions at high linear velocities in combination with no (1-5 s), medium (5-22 s), and high rotational velocities (22-23 s). As shown in the lower images, the gait sequence generator results in pure driving (blue box), hybrid static gaits (green box), i.e., one leg at a time, and hybrid trotting gaits (red box), respectively. Especially the pure driving phases reduce the COT drastically.

[10] W. Reid, F. J. Pérez-Grau, A. H. Göktoğan, and S. Sukkarieh, "Actively articulated suspension for a wheel-on-leg rover operating on a martian analog surface," in *IEEE Int. Conf. on Robotics and Automation*, 2016, pp. 5596–5602.

[11] P. R. Giordano, M. Fuchs, A. Albu-Schaffer, and G. Hirzinger, "On the kinematic modeling and control of a mobile platform equipped with steering wheels and movable legs," in *IEEE Int. Conf. on Robotics and Automation*, 2009, pp. 4080–4087.

[12] F. Cordes, C. Oekermann, A. Babu, D. Kuehn, T. Stark, F. Kirchner, and D. R. I. C. Bremen, "An active suspension system for a planetary rover," in *Proceedings of the Int. Symposium on Artificial Intelligence, Robotics and Automation in Space (i-SAIRAS)*, 2014, pp. 17–19.

[13] M. Giftthaler, F. Farshidian, T. Sandy, L. Stadelmann, and J. Buchli, "Efficient kinematic planning for mobile manipulators with non-holonomic constraints using optimal control," in *IEEE Int. Conf. on Robotics and Automation*, 2017, pp. 3411–3417.

[14] A. Suzumura and Y. Fujimoto, "Real-time motion generation and control systems for high wheel-legged robot mobility," *IEEE Transactions on Industrial Electronics*, vol. 61, no. 7, pp. 3648–3659, 2014.

[15] M. Bjelonic, C. D. Bellicoso, Y. de Viragh, D. Sako, F. D. Tresoldi, F. Jenelten, and M. Hutter, "Keep rollin' - whole-body motion control and planning for wheeled quadrupedal robots," *IEEE Robotics and Automation Letters*, vol. 4, no. 2, pp. 2116–2123, 2019.

[16] M. Bjelonic, C. D. Bellicoso, M. E. Tiryaki, and M. Hutter, "Skating with a force controlled quadrupedal robot," in *IEEE/RSJ Int. Conf. on Intelligent Robots and Systems*, 2018, pp. 7555–7561.

[17] T. Klamt and S. Behnke, "Planning hybrid driving-stepping locomotion on multiple levels of abstraction," in *IEEE Int. Conf. on Robotics and Automation*, 2018, pp. 1695–1702.

[18] G. Bellegarda and K. Byl, "Trajectory optimization for a wheel-legged system for dynamic maneuvers that allow for wheel slip," in *under review for IEEE Conf. on Decision and Control (CDC)*, 2019.

[19] M. Geilinger, R. Poranne, R. Desai, B. Thomaszewski, and S. Coros, "Skaterbots: Optimization-based design and motion synthesis for robotic creatures with legs and wheels," *ACM Transactions on Graphics (TOG)*, vol. 37, no. 4, p. 160, 2018.

[20] M. Bjelonic, P. K. Sankar, C. D. Bellicoso, H. Vallery, and M. Hutter, "Rolling in the deep – hybrid locomotion for wheeled-legged robots using online trajectory optimization," *IEEE Robotics and Automation Letters*, vol. 5, no. 2, pp. 3626–3633, 2020.

[21] M. Hutter, C. Gehring, A. Lauber, F. Gunther, C. D. Bellicoso, V. Tsounis, P. Fankhauser, R. Diethelm, S. Bachmann, M. Blösch, *et al.*, "Anymal-toward legged robots for harsh environments," *Advanced Robotics*, vol. 31, no. 17, pp. 918–931, 2017.

[22] B. Aceituno-Cabezas, C. Mastalli, H. Dai, M. Focchi, A. Radulescu, D. G. Caldwell, C. J., J. C. Grieco, F.-L. G., and C. Semini, "Simultaneous contact, gait and motion planning for robust multi-legged locomotion via mixed-integer convex optimization," *IEEE Robotics and Automation Letters*, 2017.

[23] R. Deits and R. Tedrake, "Footstep planning on uneven terrain with mixed-integer convex optimization," in *IEEE-RAS Int. Conf. on humanoid robots*, 2014, pp. 279–286.

[24] A. W. Winkler, C. D. Bellicoso, M. Hutter, and J. Buchli, "Gait and trajectory optimization for legged systems through phase-based end-effector parameterization," *IEEE Robotics and Automation Letters*, vol. 3, no. 3, pp. 1560–1567, 2018.

[25] O. Melon, M. Geisert, D. Surovik, I. Havoutis, and M. Fallon, "Reliable trajectories for dynamic quadrupeds using analytical costs and learned initializations," *IEEE Int. Conf. on Robotics and Automation*, 2020.

[26] J. Carius, R. Ranftl, V. Koltun, and M. Hutter, "Trajectory optimization for legged robots with slipping motions," *IEEE Robotics and Automation Letters*, vol. 4, no. 3, pp. 3013–3020, 2019.

[27] K. Lowrey, A. Rajeswaran, S. Kakade, E. Todorov, and I. Mordatch, "Plan online, learn offline: Efficient learning and exploration via model-based control," in *Int. Conf. on Learning Representations*, 2019. [Online]. Available: https://openreview.net/forum?id=Byey7n05FQ

[28] C. Boussema, M. J. Powell, G. Bledt, A. J. Ijspeert, P. M. Wensing, and S. Kim, "Online gait transitions and disturbance recovery for legged robots via the feasible impulse set," *IEEE Robotics and Automation Letters*, vol. 4, no. 2, pp. 1611–1618, 2019.

[29] T. Klamt and S. Behnke, "Anytime hybrid driving-stepping locomotion planning," in *Int. Conf. on Intelligent Robots and Systems*, 2017, pp. 4444–4451.

[30] V. Tsounis, M. Alge, J. Lee, F. Farshidian, and M. Hutter, "Deepgait: Planning and control of quadrupedal gaits using deep reinforcement learning," *IEEE Robotics and Automation Letters*, vol. 5, no. 2, pp. 3699–3706, 2020.

[31] Y. de Viragh, M. Bjelonic, C. D. Bellicoso, F. Jenelten, and M. Hutter, "Trajectory optimization for wheeled-legged quadrupedal robots using linearized zmp constraints," in *IEEE Robotics and Automation Letters*, 2019.

[32] J. Di Carlo, P. M. Wensing, B. Katz, G. Bledt, and S. Kim, "Dynamic locomotion in the mit cheetah 3 through convex model-predictive control," in *IEEE/RSJ Int. Conf. on Intelligent Robots and Systems*, 2018, pp. 1–9.

[33] R. Buchanan, L. Wellhausen, M. Bjelonic, T. Bandyopadhyay, N. Kottege, and M. Hutter, "Perceptive whole-body planning for multilegged robots in confined spaces," *Journal of Field Robotics*, 2020.

[34] R. Grandia, F. Farshidian, R. Ranftl, and M. Hutter, "Feedback mpc for torque-controlled legged robots," in *IEEE/RSJ Int. Conf. on Intelligent Robots and Systems*, 2019, pp. 4730–4737.

[35] M. Neunert, C. de Crousaz, F. Furrer, M. Kamel, F. Farshidian, R. Siegwart, and J. Buchli, "Fast nonlinear model predictive control for unified trajectory optimization and tracking," in *IEEE Int. Conf. on Robotics and Automation*, 2016, pp. 1398–1404.

[36] G. Bledt and S. Kim, "Implementing regularized predictive control for simultaneous real-time footstep and ground reaction force optimization," in *IEEE/RSJ Int. Conf. on Intelligent Robots and Systems*, 2019, pp. 6316–6323.

[37] M. Geilinger, S. Winberg, and S. Coros, "A computational framework for designing skilled legged-wheeled robots," *IEEE Robotics and Automation Letters*, vol. 5, no. 2, pp. 3674–3681, 2020.

[38] E. Jelavic and M. Hutter, "Whole-body motion planning for walking excavators," in *IEEE/RSJ Int. Conf. on Intelligent Robots and Systems*, 2019, pp. 2292–2299.

[39] J. Hwangbo, J. Lee, A. Dosovitskiy, D. Bellicoso, V. Tsounis, V. Koltun, and M. Hutter, "Learning agile and dynamic motor skills for legged robots," *Science Robotics*, vol. 4, no. 26, 2018.

[40] J. Carius, F. Farshidian, and M. Hutter, "Mpc-net: A first principles guided policy search," *IEEE Robotics and Automation Letters*, vol. 5, no. 2, pp. 2897–2904, 2020.

[41] M. Vukobratović and B. Borovac, "Zero-moment point – thirty five years of its life," *Int. journal of humanoid robotics*, vol. 1, no. 01, pp. 157–173, 2004.

[42] A. W. Winkler, F. Farshidian, D. Pardo, M. Neunert, and J. Buchli, "Fast trajectory optimization for legged robots using vertex-based zmp constraints," *IEEE Robotics and Automation Letters*, vol. 2, no. 4, pp. 2201–2208, 2017.

[43] G. Bellegarda, K. van Teeffelen, and K. Byl, "Design and evaluation of skating motions for a dexterous quadruped," in *IEEE Int. Conf. on Robotics and Automation*, 2018.

[44] V. S. Medeiros, E. Jelavic, M. Bjelonic, R. Siegwart, M. A. Meggiolaro, and M. Hutter, "Trajectory optimization for wheeled-legged quadrupedal robots driving in challenging terrain," *IEEE Robotics and Automation Letters*, vol. 5, no. 3, pp. 4172–4179, 2020.

[45] D. E. Orin, A. Goswami, and S.-H. Lee, "Centroidal dynamics of a humanoid robot," *Autonomous robots*, vol. 35, no. 2-3, pp. 161–176, 2013.

[46] M. H. Raibert, *Legged robots that balance*. MIT press, 1986.

[47] J. Pratt, J. Carff, S. Drakunov, and A. Goswami, "Capture point: A step toward humanoid push recovery," in *IEEE-RAS Int. Conf. on humanoid robots*, 2006, pp. 200–207.

[48] F. Farshidian, M. Neunert, A. W. Winkler, G. Rey, and J. Buchli, "An efficient optimal planning and control framework for quadrupedal locomotion," in *IEEE Int. Conf. on Robotics and Automation*, 2017, pp. 93–100.

[49] R. Grandia, F. Farshidian, A. Dosovitskiy, R. Ranftl, and M. Hutter, "Frequency-aware model predictive control," *IEEE Robotics and Automation Letters*, vol. 4, no. 2, pp. 1517–1524, 2019.

[50] A. W. Winkler, "Optimization-based motion planning for legged robots," Ph.D. dissertation, ETH Zurich, 2018.

[51] M. Bloesch, M. Hutter, M. A. Hoepflinger, S. Leutenegger, C. Gehring, C. D. Remy, and R. Siegwart, "State estimation for legged robots-consistent fusion of leg kinematics and imu," *Robotics*, vol. 17, pp. 17–24, 2013.

[52] R. Orsolino, M. Focchi, S. Caron, G. Raiola, V. Barasuol, D. G. Caldwell, and C. Semini, "Feasible region: An actuation-aware extension of the support region," *IEEE Transactions on Robotics*, vol. 36, no. 4, pp. 1239–1255, 2020.